



## Importance of meteorology in air pollution events during the city lockdown for COVID-19 in Hubei Province, Central China

Lijuan Shen <sup>a</sup>, Tianliang Zhao <sup>a,\*</sup>, Honglei Wang <sup>a,\*</sup>, Jane Liu <sup>b</sup>, Yongqing Bai <sup>c</sup>, Shaofei Kong <sup>d</sup>, Huang Zheng <sup>d</sup>, Yan Zhu <sup>a</sup>, Zuozihi Shu <sup>a</sup>

<sup>a</sup> Collaborative Innovation Center on Forecast and Evaluation of Meteorological Disasters, Key Laboratory for Aerosol-Cloud-Precipitation of the China Meteorological Administration, PREMIC, Nanjing University of Information Science & Technology, Nanjing 210044, China

<sup>b</sup> Department of Geography and Planning, University of Toronto, Toronto, Ontario M5S3G3, Canada

<sup>c</sup> Institute of Heavy Rain, China Meteorological Administration, Wuhan 430205, China

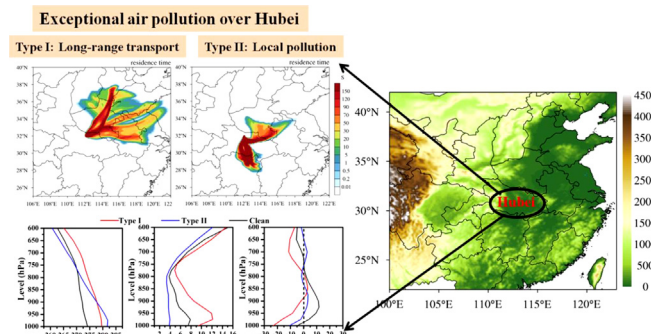
<sup>d</sup> Department of Atmospheric Sciences, School of Environmental Studies, China University of Geosciences (Wuhan), Wuhan 430074, China



### HIGHLIGHTS

- Inverse changes in AOD and AE during lockdown were found over CEC.
- Pollution events were frequently observed during the strictest lockdown over Hubei.
- Air pollution was caused by regional transport of upstream air pollutants to Hubei.
- Local pollution was accumulated despite of large reductions in air pollutant emissions.

### GRAPHICAL ABSTRACT



### ARTICLE INFO

#### Article history:

Received 25 June 2020

Received in revised form 24 August 2020

Accepted 3 September 2020

Available online 4 September 2020

#### Keywords:

COVID-19  
PM<sub>2.5</sub> pollution  
Meteorology  
FLEXPART-WRF

### ABSTRACT

Compared with the 21-year climatological mean over the same period during 2000–2020, the aerosol optical depth (AOD) and Angstrom exponent (AE) during the COVID-19 lockdown (January 24–February 29, 2020) decreased and increased, respectively, in most regions of Central-Eastern China (CEC). The AOD (AE) values decreased (increased) by 39.2% (29.4%) and 31.0% (45.3%) in Hubei and Wuhan, respectively, because of the rigorous restrictions. These inverse changes reflected the reduction of total aerosols in the air and the contribution of the increase in fine-mode particles during the lockdown. The surface PM<sub>2.5</sub> had a distinct spatial distribution over CEC during the lockdown, with high concentrations in North China and East China. In particular, relatively high PM<sub>2.5</sub> concentrations were notable in the lower flatlands of Hubei Province in Central China, where six PM<sub>2.5</sub> pollution events were identified during the lockdown. Using the observation data and model simulations, we found that 50% of the pollution episodes were associated with the long-range transport of air pollutants from upstream CEC source regions, which then converged in the downstream Hubei receptor region. However, local pollution was dominant for the remaining episodes because of stagnant meteorological conditions. The long-range transport of air pollutants substantially contributed to PM<sub>2.5</sub> pollution in Hubei, reflecting the exceptional importance of meteorology in regional air quality in China.

© 2020 Elsevier B.V. All rights reserved.

\* Corresponding authors.

E-mail addresses: [tlzhao@nuist.edu.cn](mailto:tlzhao@nuist.edu.cn) (T. Zhao), [hongleiwang@nuist.edu.cn](mailto:hongleiwang@nuist.edu.cn) (H. Wang).

## 1. Introduction

Urban agglomerations over the North China Plain (NCP), Yangtze River Middle Reaches, Yangtze River Delta (YRD), and Pearl River Delta (PRD) have been generated with rapid economic development and urbanization in China, which has resulted in air pollution problems during the past few decades (Zhang et al., 2012; Han et al., 2016; Gui et al., 2019). Haze pollution in the ambient atmosphere induced by high aerosol concentrations, especially anthropogenic fine particles with aerodynamic diameters less than or equal to  $2.5\text{ }\mu\text{m}$  ( $\text{PM}_{2.5}$ ) (Li et al., 2017), has been the most prevalent atmospheric pollution phenomenon in China (Guo et al., 2014; An et al., 2019). Considerable attention has been paid to  $\text{PM}_{2.5}$  particles because of their important roles in air quality and climate change (Tao et al., 2012; Wang et al., 2018; Zheng et al., 2015; Rosenfeld et al., 2014).

Generally, heavy haze events occur in four source regions in China: the NCP in North China, the YRD in East China, the PRD in South China, and the Sichuan Basin (SB) in Southwest China (Xu et al., 2016; Zhang et al., 2013). Governed by atmospheric circulation, the regional transport of  $\text{PM}_{2.5}$  emitted from these source regions can deteriorate air quality in the downwind receptor regions, leading to regional haze pollution in a large area across Central-Eastern China (CEC) (Li et al., 2013; Jiang et al., 2015; Bei et al., 2016; Chen et al., 2019; Wang et al., 2019). Haze pollution events in the NCP have been observed to mainly result from air pollutant accumulation under stable weather conditions in winter (Zhao et al., 2013; Gao et al., 2015; Zhang et al., 2016). The southward movement of cold fronts during the East Asian winter monsoon season, which is usually conducive to the rapid removal of atmospheric pollutants in the NCP (Zhao et al., 2013; Gao et al., 2016), can induce long-range transport of air pollutants from upwind regions to downwind regions in China (Hsu et al., 2010; Kang et al., 2019). Hubei Province in Central China, which has a distinct sub-basin terrain, is geographically located between the four haze pollution regions of the NCP, YRD, PRD, and SB, as shown in Fig. 1. As such, it may be pivotal for the regional transport of air pollutants in China driven by East Asian monsoonal winds. However, the regional transport of air pollutants across CEC forced by meteorological drivers remains to be poorly understood.

Recently, Hubei has increasingly suffered from haze pollution (Wang et al., 2014; Tan et al., 2015; Xu et al., 2017; Gao et al., 2019). Several studies concerning the air pollution in this region have been conducted (Zhang et al., 2015; Zheng et al., 2019; Bai et al., 2020). Generally, the changes of air pollutants are highly dependent on their emissions and meteorological conditions (Tie et al., 2017; Xu et al., 2016; An et al., 2019). If the regional amount of emitted air pollutants is roughly stable in a particular period, meteorological conditions may

be the determining factor for the occurrence of air pollution (Kan et al., 2012). To control the spread of the 2019 novel coronavirus (COVID-19), China launched a level-I response to this public health emergency in 30 provinces, autonomous regions, and municipalities as early as January 25, and was the first country to shut down commercial activities, restrict travel, and require its people to stay home (Tian et al., 2020; Wang et al., 2020a, 2020b). From January 24, 2020, Hubei was the first province in China to implement these restrictions, which are believed to have caused large reductions in air pollutant emissions over large regions in China (Huang et al., 2020; Chang et al., 2020; Shi and Brasseur, 2020). Such anomalies in air pollutants ( $\text{PM}_{2.5}$ ,  $\text{NO}_2$ , and  $\text{O}_3$ ) diminished near the end of February 2020, when restrictions related to COVID-19 began to be eased and people outside of Hubei province started to return to work (Huang et al., 2020; Wang et al., 2020a). However, there were still several air pollution episodes in North China (Le et al., 2020), East China (Huang et al., 2020), and especially Hubei Province of Central China, which had the strictest city lockdown measures. Thus, using comprehensive measurements of ground-based data, satellite observations, and reanalysis data, as well as model simulations, we first assess the extent of wintertime aerosol changes over CEC during the city lockdown for COVID-19 (January 24–February 29, 2020) by comparing aerosol optical depth (AOD) and Angstrom exponent (AE) values during the same period over 2000–2020, and further investigate the importance of meteorology in driving regional transport and accumulation of air pollutants with respect to air quality change in Hubei under the rare low emissions of anthropogenic pollutants over a large region in China.

## 2. Data and methods

### 2.1. Data

The Moderate Resolution Imaging Spectroradiometer (MODIS) is a sensor aboard NASA's TERRA satellite with 36 bands from 0.4 to  $14.4\text{ }\mu\text{m}$ , a relatively fine spatial resolution between 250 and 1000 m, and a wide range of  $\sim 2330$  km. This sensor can act as a feasible means of land aerosol remote-sensing (Chu et al., 2002). This study used Terra MODIS C6.1 Level 2 aerosol products (MOD04\_L2) at 10 km spatial resolution from 2000 to 2020. All data were downloaded from NASA Level 1 and the Atmosphere Archive and Distribution System (<https://ladsweb.nascom.nasa.gov/data/search.html>). The Dark Target merged AOD data at 550 nm (hereafter referred to as AOD) were principally used in this study. The AE provided information about the dominant particle size in the atmospheric column, which was calculated using the linear fit of AOD against  $\lambda$  on a logarithmic scale; thus, the AE between 470 and 660 nm ( $\text{AE}_{470-660}$ ) product was used to study the dominance of fine-mode particles over CEC.

Hourly  $\text{PM}_{2.5}$  concentrations used in this study were derived from the public data of the Ministry of Ecology and Environment of China (<http://106.37.208.233:20035/>), including more than 1600 ambient air quality monitoring stations across China. The  $\text{PM}_{2.5}$  concentrations were measured by the micro-oscillating balance method and the  $\beta$  absorption method, following the China Environmental Protection Standards HJ 93-2013 and HJ 655-2013 (<http://www.cnemc.cn/jcgf/dqjhj/201711/P020181010540081577412.pdf>). Smooth  $\text{PM}_{2.5}$  concentration maps were further obtained by gridding these point data with the Cressman interpolation method (An et al., 2020; Shen et al., 2020). The regional averages of  $\text{PM}_{2.5}$  mass concentrations obtained from the total monitoring sites over Hubei, China, were chosen for the  $\text{PM}_{2.5}$  pollution analysis. The chemical components in  $\text{PM}_{2.5}$  were determined using on-line instruments at an environmental monitoring supersite in Wuhan ( $114.38^\circ\text{E}, 30.52^\circ\text{N}$ ).

The reanalysis data for 2000–2019 used to calculate the climatological wind field were provided by the National Center for Environmental Prediction (NCEP, <https://www.ncep.noaa.gov/>), with a horizontal resolution of  $1^\circ \times 1^\circ$ . Horizontal and vertical meteorological data of air

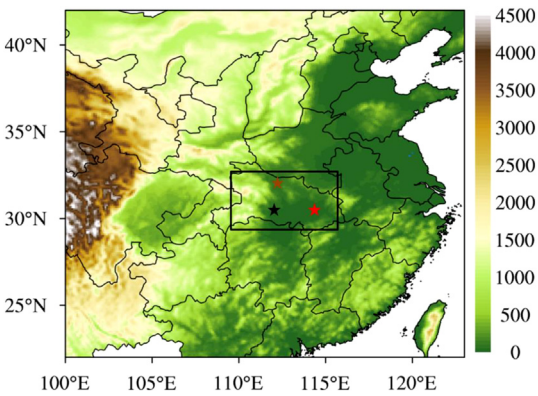


**Fig. 1.** Distribution of terrain heights (m; a.s.l.) over Central-Eastern China. The black box marks the region of Hubei Province, and the red, brown and black star indicate the locations of three urban sites Wuhan (WH), Xiangyang (XY) and Jingzhou (JZ) in Hubei Province, respectively.

temperature and wind speed during the pollution episodes were obtained from the MERRA-2 reanalysis dataset with a horizontal resolution of  $0.5^\circ \times 0.625^\circ$  (<https://disc.gsfc.nasa.gov/datasets?project=MERRA-2>). Observational data of meteorology including hourly surface air temperature, relative humidity (RH), precipitation, and near-surface wind speed and direction in Hubei were obtained from the national weather monitoring network of the China Meteorological Administration.

## 2.2. FLEXPART-WRF model

The WRF model provides the fine meteorological fields driving the FLEXPART model during pollution events. In this study, the WRF model was configured with two nested domains, coarse and fine. The coarse domain covered the entirety of Asia with a  $30 \times 30$  km horizontal resolution, and the nested fine domain included most of China and its surrounding regions with a  $10 \times 10$  km horizontal resolution. The physical parameterizations used in WRF modeling were the Morrison micro-physics scheme (Morrison et al., 2009), Rapid Radiative Transfer Model (RRTM) scheme for long- and short-wave radiation (Milawer et al., 1997), Yonsei University (YSU) boundary layer scheme (Hong et al., 2006), Grell 3D cumulus parameterization, and Noah land surface scheme (Grell et al., 2005). Using the reanalysis meteorological data in the horizontal resolution of  $1^\circ \times 1^\circ$  obtained from the NCEP for initial and boundary meteorological conditions, the WRF simulation ran for 12 h each time, where the first 6 h of simulations constituted spin-up time.

A Lagrangian particle dispersion model, FLEXPART-WRF version 3.1 (Brioude et al., 2013; Stohl et al., 2005; Fast and Easter, 2006), was used to determine the origin and transport pathways of particles arriving at the receptor site. In this model, the trajectories of a large number of particles released from a source are simulated, considering the processes of tracer transport, turbulent diffusion, and wet and dry deposition in the atmosphere (Brioude et al., 2013); thus, it simulates the transport and dispersion of tracers by calculating the backward trajectories of multitudinous particles, which are termed plume backward trajectories, reflecting the distribution of potential source regions that may have impacts on a target point or receptor region (Chen et al., 2017; Seibert and Frank, 2004; Zhai et al., 2016).

To improve the accuracy of the trajectory calculation, we used high-resolution WRF simulation domain 2 outputs as the input meteorological conditions for the FLEXPART model, which has been widely used to investigate the potential sources of air pollutants in relation to environmental change (Stohl, 2003; Gadhavi et al., 2015; Sauvage et al., 2017; Zhu et al., 2018). In this study, the FLEXPART-WRF simulation was conducted for a 24-hour backward trajectory with the release of 10,000 air particles in the first hour from Xiangyang (XY,  $32.0^\circ\text{N}$ ,  $112.1^\circ\text{E}$ ), Wuhan (WH,  $30.6^\circ\text{N}$ ,  $114.3^\circ\text{E}$ ), and Jingzhou (JZ,  $30.3^\circ\text{N}$ ,  $112.2^\circ\text{E}$ ), respectively, for six pollution events during the lockdown. The output domain in FLEXPART-WRF was set up with six vertical levels (10, 100, 500, 1000, 2000, and 4000 m) with a 10–1000 km release height and a horizontal resolution of  $0.1^\circ \times 0.1^\circ$ .

## 3. Results and discussion

### 3.1. AOD and AE anomalies over CEC

High AOD values exceeding 0.5 existed over CEC, revealing regional aerosol pollution during 2000–2020 (Fig. 2a). In particular, higher AOD values ( $>0.9$ ) were observed over the lower flatland of Hubei and Hunan provinces, based on comparisons of Figs. 1 and 2a, which highlighted an area of aerosol pollution in Central China (Shen et al., 2020). Comparison of AOD and AE between the averages during the lockdown and the 21-year climatological mean over the same period during 2000–2020 presented distinct anomalous changes over CEC (Fig. 2). A large scale of negative anomalies for AOD during

lockdown was noted (Fig. 2b), revealing great impacts of the lockdown policy on the reduction in aerosol loads over CEC. However, several positive anomalies of AOD were still observed in North China, which were mostly related to the formation of severe haze caused by unfavorable meteorological conditions, invigorated heterogeneous chemistry, and enhanced secondary aerosol formation (Le et al., 2020). As satellite retrieval data, the AOD is related to surface particles as well as other factors, such as moisture content in the air (Shen et al., 2020), which may result in contrast increase of AOD values in dot areas, such as Dongting Lake in Hunan Province, Poyang Lake in Jiangxi Province, and Chaohu Lake in Anhui Province (Fig. 2b, c). Compared with the averages during 2000–2020, AOD values decreased noticeably over CEC, mostly exceeding 20% (Fig. 2c); Hubei Province and the urban site of Wuhan had greater AOD reductions by 39.2% and 31.0%, respectively, during the lockdown, which confirms the significant reductions in atmospheric aerosols.

AE can provide qualitative information on aerosol size; high values of AE indicate the dominance of fine-mode particles. Combined with the topographic data in Fig. 1, AE values exceeding 1.2 were identified in mountain areas over CEC, indicating dominant fine-mode particles in clean air regions (Shen et al., 2020). AE anomalies during the lockdown exhibited an opposite distribution compared with AOD anomalies (Fig. 2e); positive anomalies of AE in most regions of CEC indicated an enhanced contribution of fine-mode particles in the air. Overall, AE values increased by more than 15% in CEC during the lockdown compared with the climatological mean (Fig. 2f), and were enhanced by 29.4% and 45.3% in Hubei and Wuhan, respectively. Such inverse change reflected the reduction of total aerosols in the air and the increase in the contribution of fine-mode particles during the lockdown.

### 3.2. $\text{PM}_{2.5}$ distributions over CEC

Although large reductions in aerosols were observed during the COVID-19 shutdown as mentioned above, surface  $\text{PM}_{2.5}$  concentrations averaged during the city lockdown had a distinct spatial distribution over CEC (Fig. 3). High concentrations of  $\text{PM}_{2.5}$  exceeding  $65 \mu\text{g} \cdot \text{m}^{-3}$  were found in most regions of Henan in Central China and Hebei, Shanxi, Shaanxi, Shandong in North China. Northern Anhui and Jiangxi in East China also showed comparatively high  $\text{PM}_{2.5}$  values larger than  $45 \mu\text{g} \cdot \text{m}^{-3}$ . In particular, relatively high  $\text{PM}_{2.5}$  concentrations were observed in the lower flatlands of Hubei Province in Central China (Figs. 1 and 3), reflecting exceptional air pollution despite large reductions in primary pollutant emissions. Meanwhile, South China had relatively clean air quality with  $\text{PM}_{2.5}$  concentrations mostly below  $35 \mu\text{g} \cdot \text{m}^{-3}$ .

#### 3.2.1. $\text{PM}_{2.5}$ pollution events in Hubei during lockdown

Fig. 4 shows that the  $\text{PM}_{2.5}$  concentration in Hubei during the lockdown ranged from  $9.5$  to  $99.3 \mu\text{g} \cdot \text{m}^{-3}$  with an average of  $46.6 \mu\text{g} \cdot \text{m}^{-3}$ , much lower than the average level during same period in 2019 ( $74.2 \mu\text{g} \cdot \text{m}^{-3}$ ). Although there were significant reductions in aerosol loads and surface  $\text{PM}_{2.5}$  concentrations during the lockdown (Zheng et al., 2020), several  $\text{PM}_{2.5}$  pollution episodes still occurred in Hubei, as shown in Fig. 4. Six  $\text{PM}_{2.5}$  pollution events had hourly concentrations larger than  $75 \mu\text{g} \cdot \text{m}^{-3}$ , and  $\text{PM}_{2.5}$  reached maximum concentrations of  $94.1$ ,  $81.2$ ,  $88.1$ ,  $89.2$ ,  $99.3$ , and  $84.8 \mu\text{g} \cdot \text{m}^{-3}$  at 06:00 January 25, 02:00 February 1, 02:00 February 2, 23:00 February 3, 12:00 February 5, and 22:00 February 25, 2020, respectively, which were  $2.0$ ,  $1.7$ ,  $1.9$ ,  $1.9$ ,  $2.1$ , and  $1.8$  times higher than the average during the lockdown.

Based on the synoptic conditions on these six pollution events with the NCEP reanalysis data of meteorology, similar configurations of atmospheric circulation conditions occurred over CEC during the pollution episodes of P1, P5, and P6, and conditions over CEC, especially Hubei Province in Central China, were controlled by a high pressure system after the passage of a cold front, with relatively large pressure gradients and prevailing strong northerly winds, which could drive the

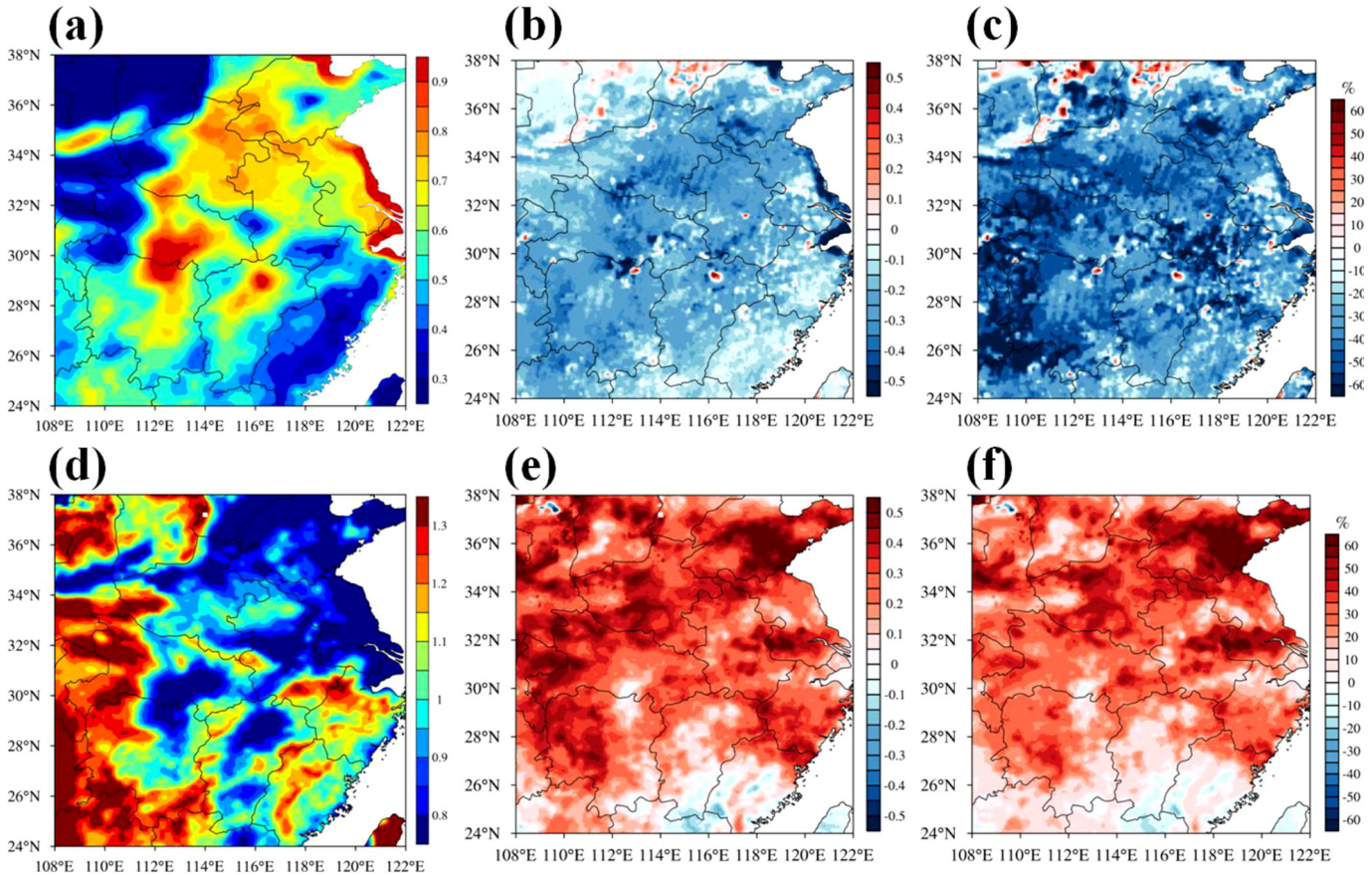


**Fig. 2.** Changes of AOD (upper) and AE (lower) during the city lockdown of COVID-19 over the CEC region. (a,d) distributions of AOD/AE averages over the same period during 2000–2020, (b,e) anomalies and (c,f) the change rates (%) of anomalies during the city lockdown relative to the averages over the same period during 2000–2020.

regional transport of air pollutants from North China to Hubei Province (Fig. S1). In contrast, the pollution processes of P2, P3, and P4 generally occurred when a uniform air pressure field existed over CEC with a weak surface pressure gradient and low wind speeds (Fig. S1), which could induce air pollutant accumulation in Hubei Province.

During the lockdown period, the near-surface meteorological factors varied greatly (Fig. 5). The wind speed had an average value of  $2.1 \text{ m} \cdot \text{s}^{-1}$ , ranging from  $0.8 \text{ m} \cdot \text{s}^{-1}$  to  $6.4 \text{ m} \cdot \text{s}^{-1}$ . The RH and air temperature fluctuated in the ranges of 24.8–98.2% and  $-0.4^\circ\text{C}$ – $20.7^\circ\text{C}$

with averages of 78.1% and  $8.0^\circ\text{C}$ , respectively. In contrast to the pollution events of P1, P5, and P6, scarce precipitation was observed for P2, P3, and P4. Notably, the wind speeds showed distinguishing changes during the six episodes, with higher speeds exceeding  $3.4 \text{ m} \cdot \text{s}^{-1}$  during P1, P5, and P6 but lower speeds below  $2.6 \text{ m} \cdot \text{s}^{-1}$  for P2, P3, and P4. Compared with the twenty-year climatology (2000–2019), anomalous northerly/easterly winds at 10 m prevailed in the lower flatland of Hubei during P1, P5, and P6 (Fig. S2). Generally, strong winds favor the purging of air pollutants (Wei et al., 2015; Yang et al., 2015). However,  $\text{PM}_{2.5}$  pollution persisted over Hubei, highlighting the possibility of the transport of  $\text{PM}_{2.5}$  from upwind regions to Hubei, given the strong northerly wind. In contrast with episodes P1, P5, and P6, negative anomalies of wind speeds were noted for P2, P3, and P4, indicating a distinct pollution pattern for these three events. Therefore, the six pollution episodes were divided into type I (including P1, P5, and P6) and type II (P2, P3, and P4) for the following discussion.

### 3.3. Reasons for two $\text{PM}_{2.5}$ pollution types

Although all the provinces in CEC went into lockdown during the same time period, the regional meteorological conditions led to accumulation of  $\text{PM}_{2.5}$  air pollution over the northern region of CEC (Fig. 6). From the observation data, it is apparent that the upwind regions of Hubei were the most polluted areas with high  $\text{PM}_{2.5}$  concentrations ( $>120 \mu\text{g} \cdot \text{m}^{-3}$ ) 24 h before the type I pollution occurred (Fig. 6a, b, c); these pollution parcels moved southward with the northerly winds (Fig. 6d, e, f) and finally reached Hubei (Fig. 6g, h, i), where the  $\text{PM}_{2.5}$  concentration increased significantly with time. These upstream regions therefore were likely the main contributor to the regional  $\text{PM}_{2.5}$  pollution over Hubei for type I episodes.

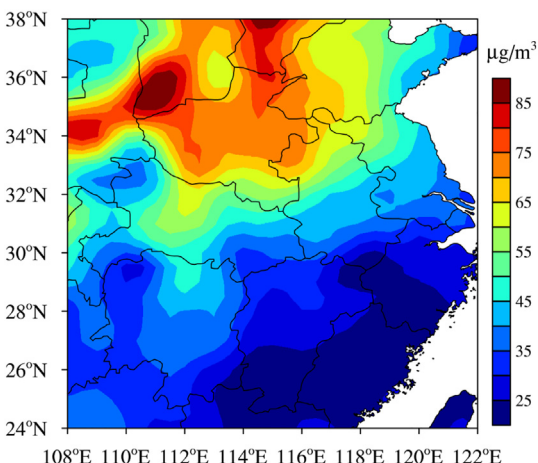


**Fig. 3.** Spatial distribution of surface  $\text{PM}_{2.5}$  concentrations over the CEC region averaged during the city lockdown.

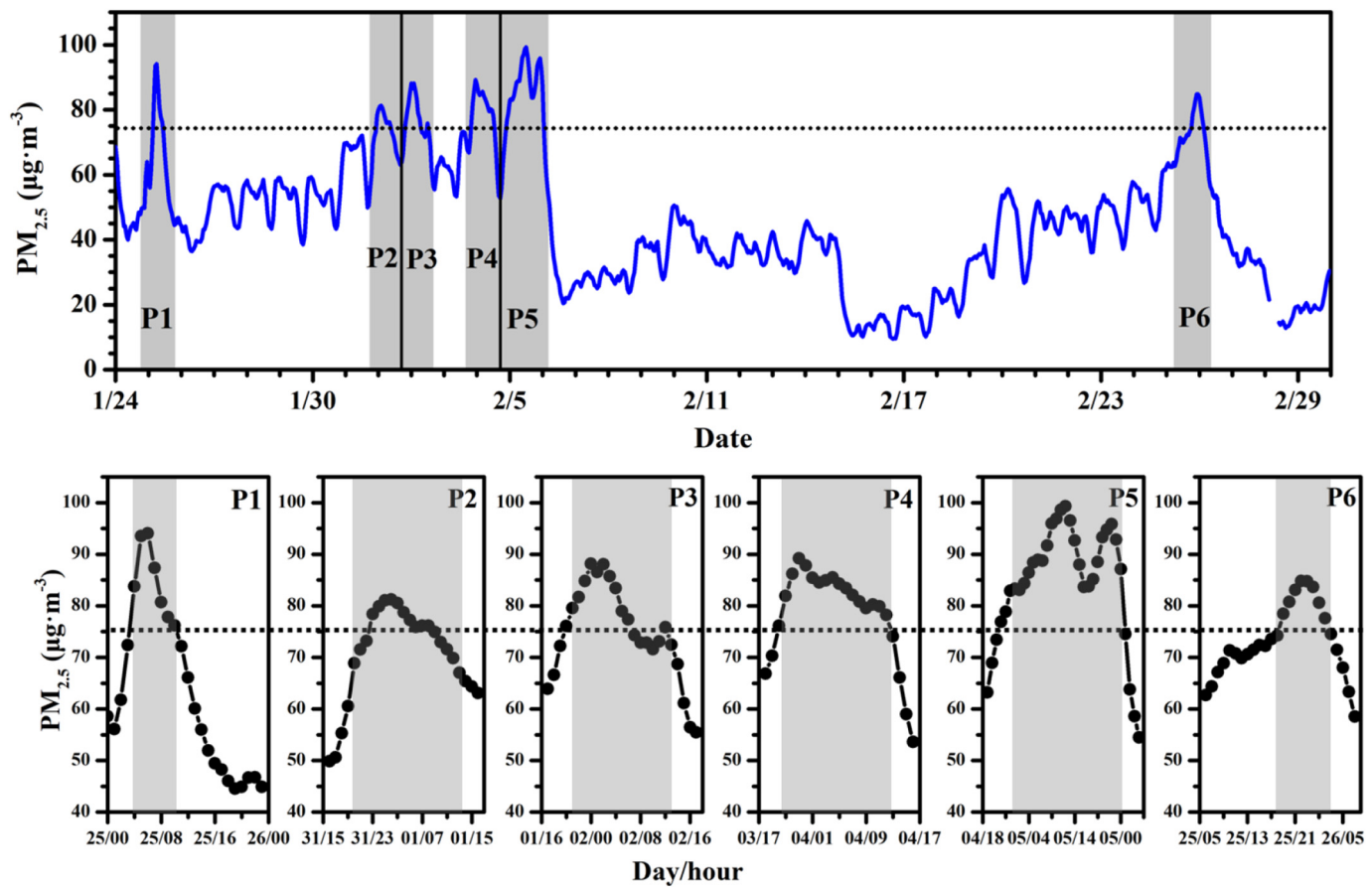


**Fig. 4.** Hourly changes of  $\text{PM}_{2.5}$  concentrations in Hubei Province during the city lockdown period with the  $\text{PM}_{2.5}$  pollution level exceeding  $75 \mu\text{g}\cdot\text{m}^{-3}$  (dash line). Six pollution events are shaded.

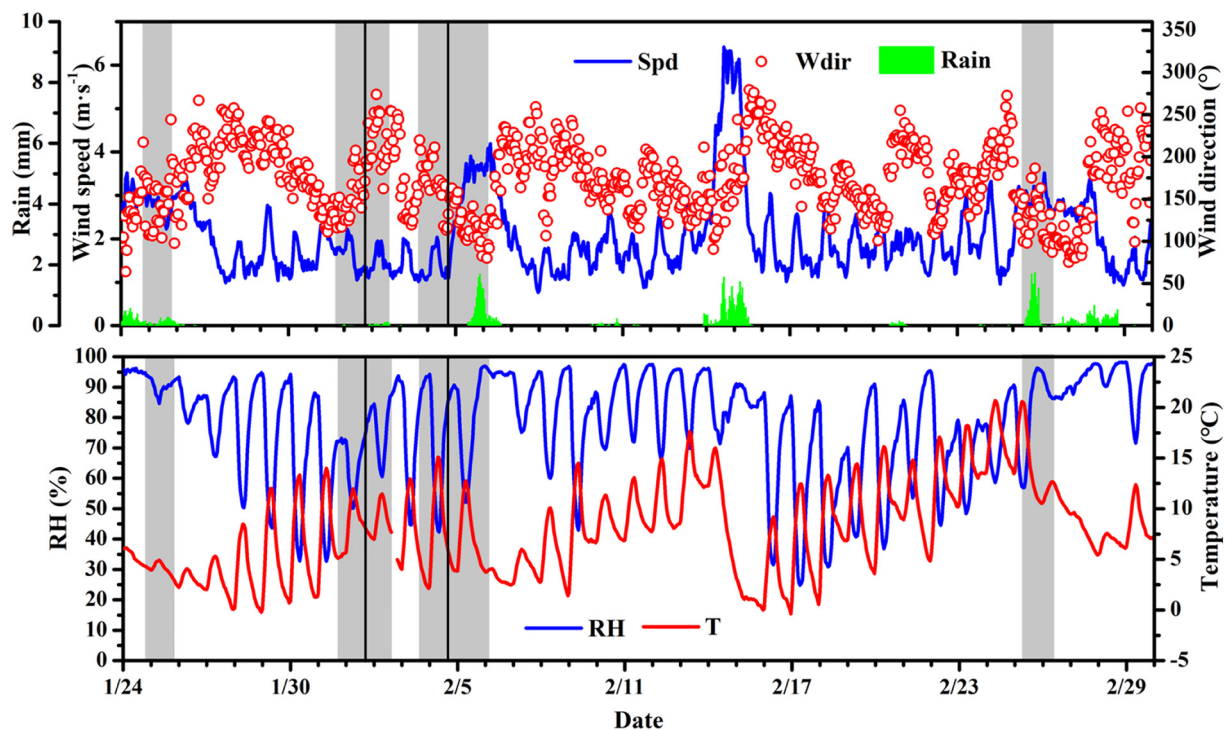
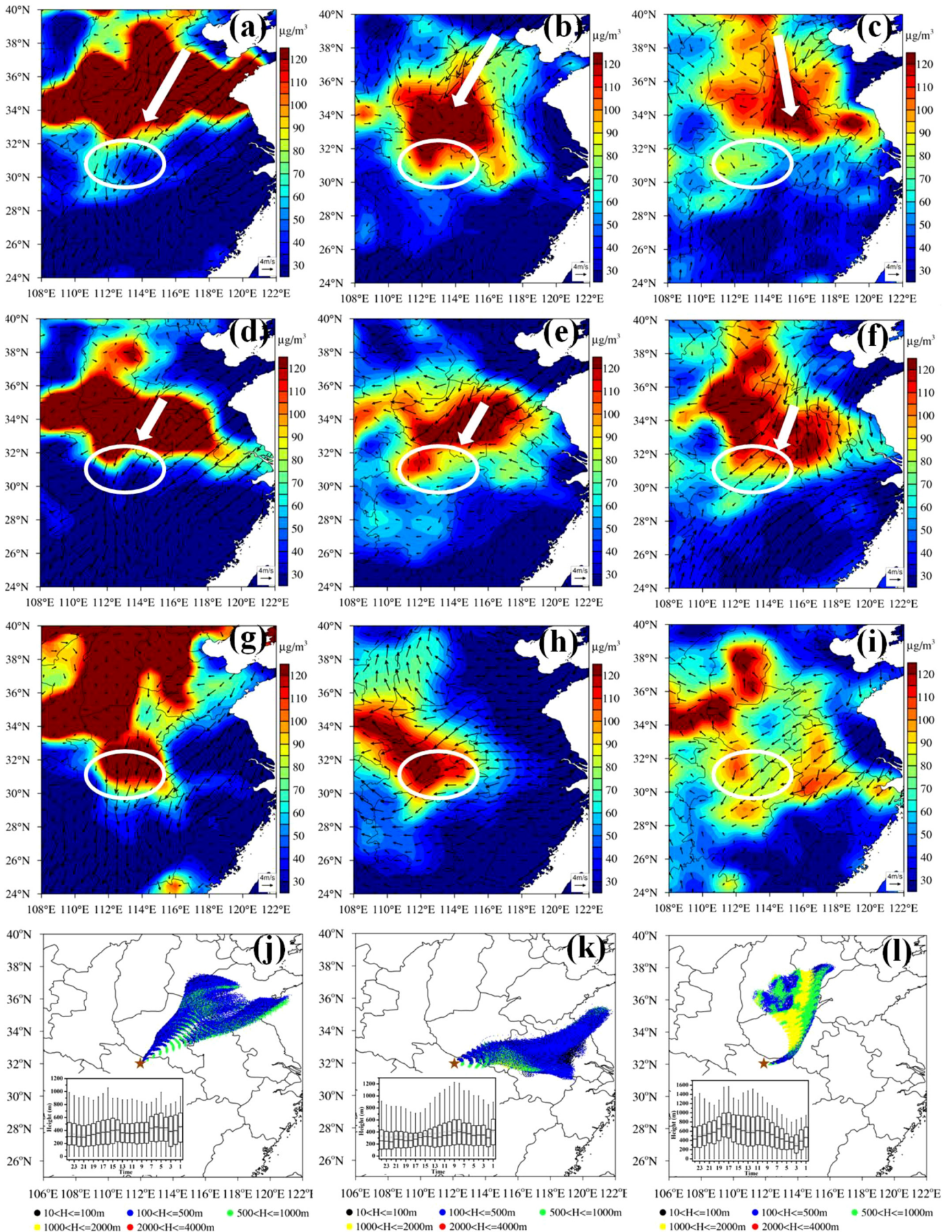


**Fig. 5.** Hourly changes of near-surface meteorological elements including wind speed (Spd), wind direction (Wdir), rain, relative humidity (RH) and air temperature (T) in Hubei Province during the city lockdown period.



The FLEXPART-WRF model simulated the explicit particle trajectories for this pollution type, which were characterized by long-range transport patterns for XY, WH, and JZ (Fig. 6j, k, l, Fig. S3). The three receptor sites were located in northwestern, eastern, and southwestern Hubei, respectively, which can roughly reflect the transport pattern of particles in the lower flatland of Hubei, and XY was the most polluted site. The same potential source regions were found for the three sites. The regional transport of air pollutants was centered along a northeastern route from Hebei in North China and the YRD in East China during P1 (Fig. 6j, Figs. S3a, d). The YRD emission sources of air pollutants exerted a considerable impact on P2 through regional transport of PM<sub>2.5</sub> across Eastern China to Hubei (Fig. 6k, Figs. S3b,e). During P6, the regional transport pathways of PM<sub>2.5</sub> from the NCP regions contributed to the elevated PM<sub>2.5</sub> concentrations (Fig. 6l, Figs. S3c, f). The transport height was limited to a low level with an average at around 400 m for P1. In contrast to P1, P6 had higher transport heights, with averages of 544, 625, and 947 m for XY, WH, and JZ, respectively, accompanied by notable sinking motions. However, the air particles were transported at lower heights (~360 m) for XY and greater heights (~730 m) for WH and JZ during P5. The discrepancy in transport heights for different sites in Hubei may have resulted from terrain effects, which should be investigated in future studies. Driven by northerly winds of the East Asian winter monsoon over CEC, the long-range transport of PM<sub>2.5</sub> from the upstream northern region to downwind in Hubei Province played a key role in the formation of type I air pollution episodes. The exceptional importance of meteorology was noted in the PM<sub>2.5</sub> accumulations over the northern region of CEC and the regional transport of PM<sub>2.5</sub> over CEC.

In contrast with the type I episodes, the type II episodes were associated with weak wind speeds and scarce rainfall when the pollution occurred (Figs. 5, 7a–c), revealing the likely role of local PM<sub>2.5</sub> accumulation over Hubei. Short plumes of tracer particles and higher traveling heights (averaging 550–1193 m) compared with type I were also shown for type II by the FLEXPART-WRF model (Fig. 7d–f, Fig. S4). Given the comparatively low PM<sub>2.5</sub> concentrations in southern Hubei (Figs. 3, 7a–c), the prevailing southerly plumes for this pollution type revealed the impacts of local PM<sub>2.5</sub> pollution over Hubei. Therefore, the stagnant conditions that caused these episodes had to cover areas in Hubei and neighboring Hunan Province, where human activities were likely shut down during the city lockdown for COVID-19 in China. Additionally, areas within 380 km from the center of XY, WH, and JZ can cover most of Hubei and Hunan provinces in Central China; therefore, a threshold of 380 km was set to distinguish local and long-range transport of pollution, based on a previous study (Hu et al., 2018). Particle plumes associated with type II were basically smaller than this threshold. Therefore, local air pollutants were dominant for type II, with tracer particles traveling at comparatively greater heights and descending obviously when the receptor sites were reached.

The increased contribution of fine-mode particles during the lockdown may have been responsible for local pollution. The major chemical components of PM<sub>2.5</sub> in WH varied significantly during the two pollution types (Fig. S5). Compared with the averages during the lockdown, the concentrations of secondary inorganic matter (SO<sub>4</sub><sup>2-</sup>, NO<sub>3</sub><sup>-</sup>, and NH<sub>4</sub><sup>+</sup>) were increased by 85.9–152.4% and 76.1–114.2% during type I and type II pollution episodes, respectively, and organic carbon concentrations increased by 0.7–103.4% and 28.0–102.8%, respectively, which confirmed the enhanced formation of secondary PM<sub>2.5</sub> during the local pollution events, separate from the regional transport processes (Chang et al., 2020). Static weather conditions and scarce rainfall in Hubei were the main drivers of secondary pollution during type II episodes. A related study also found increased amounts of sulfate, organic

carbon, and secondary inorganic aerosols in WH during the lockdown (Zheng et al., 2020). Huang et al. (2020) revealed that haze events during the COVID-19 lockdown in East China were driven by increases in atmospheric oxidizing capacity, which in turn facilitated secondary pollution.

It is worth noting that the inversion layer of air temperature did not exist during clean and type I periods (Fig. 8), whereas the type II periods had temperature inversion below 975 hPa, revealing stable weather conditions near the surface that inhibited the vertical diffusion of air pollutants. Compared with the clean air period, the type I pollution episodes were characterized by stronger winds, which increased sharply to a maximum of 12.1 m·s<sup>-1</sup> at 975 hPa and then decreased with increasing altitude at 975–775 hPa. Based on previous criteria for low-level jets (LLJs) given by Bonner (1968) and Wei et al. (2013), a LLJ in this study required V<sub>max</sub> ≥ 10 m·s<sup>-1</sup> and a corresponding falloff ΔV (V<sub>max</sub> – V<sub>min</sub>) ≥ V<sub>max</sub>/2 in the lowest 3000 m. Such vertical structures of horizontal winds with LLJs occurring during type I episodes could induce the downward mixing of regionally transported air pollutants. In contrast with type I, the type II pollution episodes had much weaker wind speeds compared with the clean periods, which were favorable to the local accumulation of air pollutants accompanied by the inversion layer. In addition, wind convergence for the two pollution types, especially type I with greater convergence in a thicker layer (Fig. 8), promoted the accumulation of PM<sub>2.5</sub> near the surface of Hubei with elevated ambient PM<sub>2.5</sub> concentrations, thus contributing to air pollution.

Based on comparisons of the average concentrations during the lockdown and the two pollution types, positive anomalies of PM<sub>2.5</sub> were identified in the lower flatland of Hubei during type I episodes (Fig. S6), whereas the upstream regions generally featured negative anomalies of PM<sub>2.5</sub> concentrations, affirming the regional transport of PM<sub>2.5</sub> from the upstream CEC source regions to the downstream Hubei receptor region. However, type II was characterized by positive anomalous PM<sub>2.5</sub> concentrations across CEC centered in Hubei, reflecting the impact of stagnant meteorological conditions on the local pollution, especially in the sub-basin of Hubei, during type II events (Fig. 7, Figs. S1, S2 and S6). By dividing the air pollution anomalies by the lockdown averages of PM<sub>2.5</sub> concentrations observed in Hubei, it was estimated that the PM<sub>2.5</sub> concentrations increased by 79.8–96.1% and 75.5–82.6% during type I and type II episodes, respectively; therefore, the long-range transport of air pollutants contributed more to PM<sub>2.5</sub> pollution in Hubei.

#### 4. Conclusions

This study demonstrated the impacts of regional transport vs. local emission sources by examining an unprecedented period when human activities were largely shut down in Hubei Province, Central China. Compared with the 21-year climatological mean over the same period during 2000–2020, the AOD and AE values during the city lockdown for COVID-19 decreased and increased, respectively; in most regions of CEC, AOD (AE) values decreased (increased) by 39.2% (29.4%) and 31.0% (45.3%) in Hubei and Wuhan, respectively, because of the rigorous restrictions. Such inverse changes reflected the reduction of total aerosols in the air and the contribution of the increase in fine-mode particles during the lockdown.

Although large reductions in aerosols were observed during the lockdown, the surface PM<sub>2.5</sub> had a distinct spatial distribution over CEC, with high PM<sub>2.5</sub> concentrations in North China and East China. In particular, relatively high PM<sub>2.5</sub> concentrations were notable in the

**Fig. 6.** Distributions of surface PM<sub>2.5</sub> concentrations (color contours) and 10 m wind vectors 24-h, 12-h before and during type I of PM<sub>2.5</sub> pollution periods (P1:a,d,g; P5:b,e,h; P6: c,f,i) and the 24-h backward trajectory of air particles at different heights in XY (P1:j; P5: k; P6:l). The insert figures in j, k,l refer to the time series of plume particle heights, the lower and higher tentacles, the upper and lower edges of box, and the square and horizontal line in box indicate the minimum and maximum, 25th and 75th percentiles, and mean and median of particle heights, respectively.

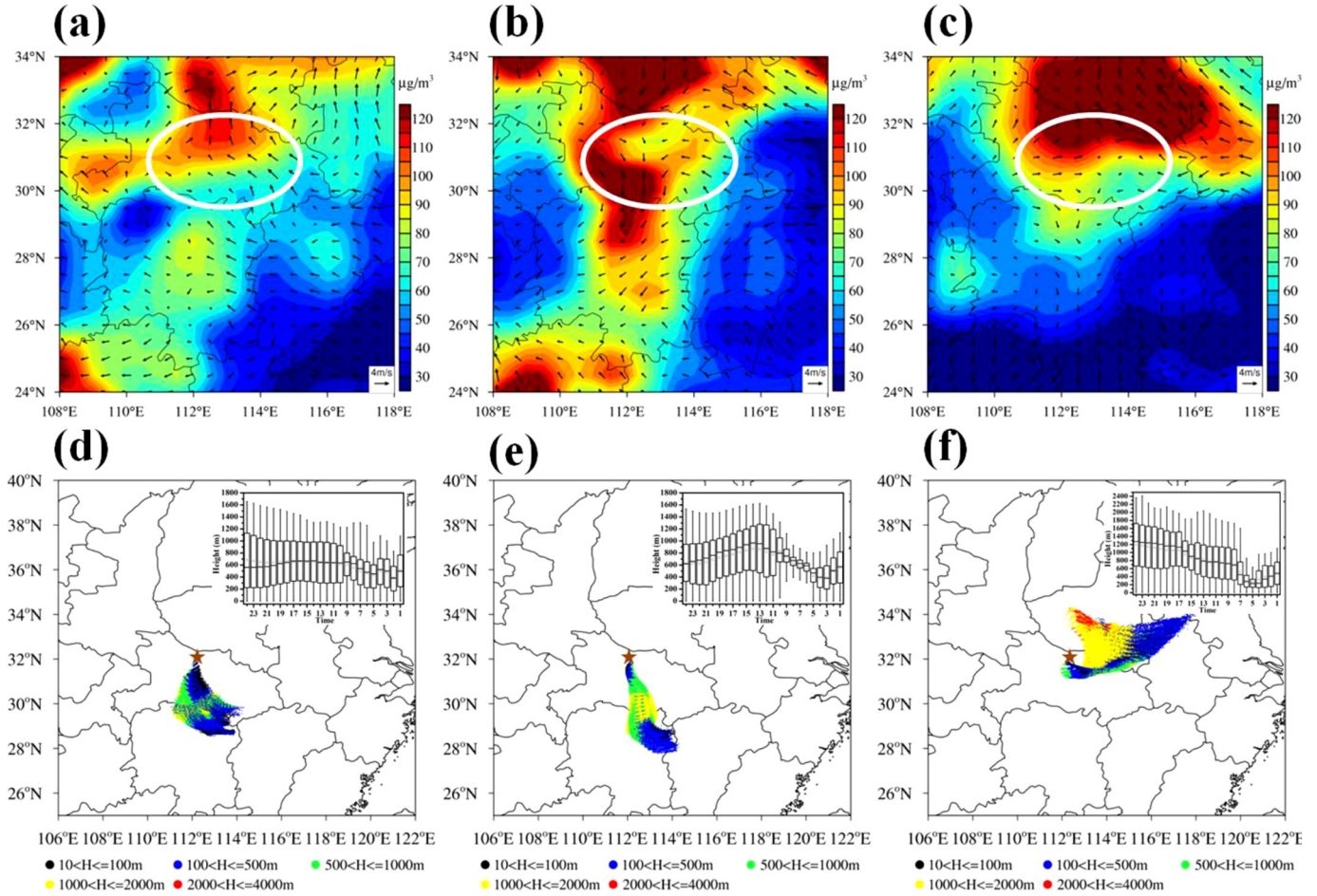


**Fig. 7.** Distributions of surface PM<sub>2.5</sub> concentrations (color contours) and 10 m wind vectors during type II of PM<sub>2.5</sub> pollution periods (P2;a; P3;b; P4;c) and the 24-hbackward trajectory of particles at different heights in XY (P2;d; P3;e; P4;f). The insert figures in d, e, f refer to the time series of plume particle heights, the lower and higher tentacles, the upper and lower edges of box, and the square and horizontal line in box indicate the minimum and maximum, 25th and 75th percentiles, and mean and median of particle heights, respectively.

lower flatlands of Hubei in Central China, where six exceptional PM<sub>2.5</sub> pollution events were detected with hourly concentrations higher than 75 µg·m<sup>-3</sup>. Anomalous northerly/easterly winds at 10 m prevailed during P1, P5, and P6, representing type I pollution, whereas negative anomalies of wind speed were noted for P2, P3, and P4, which were classified as type II pollution. Type I was characterized by the long-range

transport of air pollutants from upstream CEC source regions, which then converged in the downstream Hubei receptor region, whereas local air pollutants were dominant for type II because of stagnant meteorological conditions despite large reductions in primary pollutants. It was calculated that the PM<sub>2.5</sub> concentrations increased by 79.8–96.1% and 75.5–82.6% during type I and type II pollution episodes,

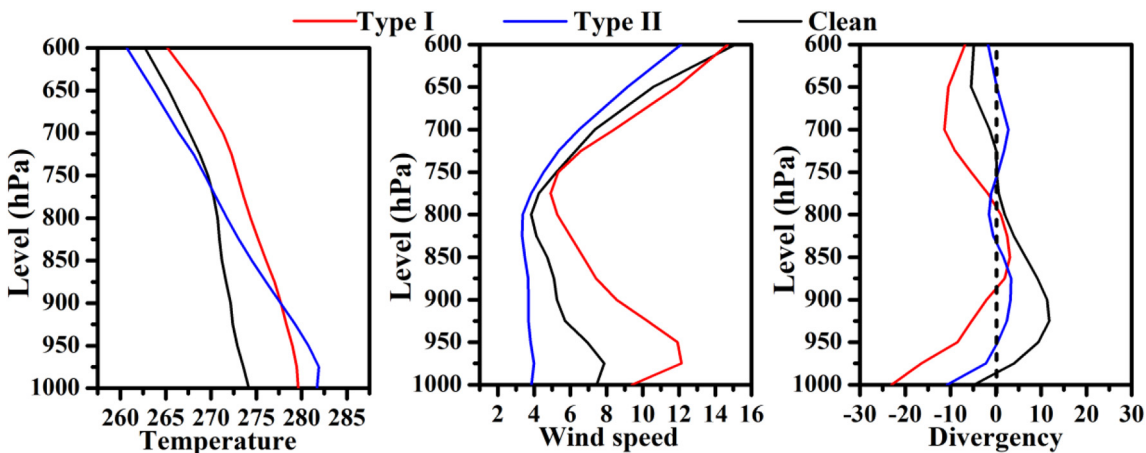


**Fig. 8.** Vertical profiles of air temperature (°C), wind speed (m·s<sup>-1</sup>) and wind divergence (10<sup>-6</sup> s<sup>-1</sup>) during type I, type II pollution and clean period during the city lockdown period in Hubei Province.

respectively, compared with the averages in Hubei during the lockdown; therefore, the long-range transport of air pollutants contributed more to PM<sub>2.5</sub> pollution in Hubei.

This study revealed the exceptional importance of meteorological drivers for air quality change under the rare low emissions of anthropogenic pollutants during the COVID-19 lockdown over a large region in China; these results imply the difficulty of air pollution mitigation under the anomalous changes of meteorology over the Asian monsoon regions.

## Author contributions

Lijuan Shen, Tianliang Zhao, Honglei Wang and Jane Liu conceived and designed the experiments as well as wrote the article; Yongqing Bai, Shaofei Kong, Huang Zheng, Yan Zhu and Zhuozhi Shu involved in the discussions and helped in the data analysis.

## Declaration of competing interest

We declare that we have no financial and personal relationships with other people or organizations that can inappropriately influence our work, there is no professional or other personal interest of any nature or kind in any product, service and/or company that could be construed as influencing the position presented in, or the review of, the manuscript entitled "**Exceptional importance of meteorology in air pollution events during the city lockdown of COVID-19 over Hubei Province of Central China**".

## Acknowledgments

This research was supported by the National Key R&D Program Pilot Projects of China (2016YFC0203304) and the National Natural Science Foundation of China (41830965, 91644223, and 91744209).

## Appendix A. Supplementary data

Supplementary data to this article can be found online at <https://doi.org/10.1016/j.scitotenv.2020.142227>.

## References

- An, Z., Huang, R.J., Zhang, R., Tie, X., Li, G., Cao, J., Zhou, W., Shi, Z., Han, Y., Gu, Z., Ji, Y., 2019. Severe haze in Northern China: a synergy of anthropogenic emissions and atmospheric processes. *P. Natl. Acad. Sci. U.S.A.* 116 (18), 8657–8666.
- An, X., Sheng, L., Liu, Q., Li, C., Gao, Y., Li, J., 2020. The combined effect of two westerly jet waveguides on heavy haze in the North China Plain in November and December 2015. *Atmos. Chem. Phys.* 20 (8), 4667–4680.
- Bai, D., Wang, H., Tan, Y., Yin, Y., Wu, Z., Guo, S., Shen, L., Zhu, B., Wang, J., Kong, X., 2020. Optical properties of aerosols and chemical composition apportionment under different pollution levels in Wuhan during January 2018. *Atmosphere* 11 (1), 17.
- Bei, N., Xiao, B., Meng, N., Feng, T., 2016. Critical role of meteorological conditions in a persistent haze episode in the Guanzhong basin, China. *Sci. Total Environ.* 550, 273–284.
- Bonner, W.D., 1968. Climatology of the low level jet. *Mon. Weather Rev.* 96 (12), 833–850.
- Brioude, J., Arnold, D., Stohl, A., Cassiani, M., Morton, D., Seibert, P., Angevine, W., Evan, S., Dingwell, A., Fast, J.D., Easter, R.C., Pisso, I., Burkhardt, J., Wotawa, G., 2013. The Lagrangian particle dispersion model FLEXPART-WRF version 3.1. *Geosci. Model Dev.* 6, 1889–1904. <https://doi.org/10.5194/gmd-6-1889-2013>.
- Chang, Y., Huang, R.J., Ge, X., Huang, X., Hu, J., Duan, Y., Zou, Z., Liu, X., Lehmann, M.F., 2020. Puzzling haze events in China during the coronavirus (COVID-19) shutdown. *Geophys. Res. Lett.* 47, 11.
- Chen, B., Xu, X.D., Zhao, T., 2017. Quantifying oceanic moisture exports to mainland China in association with summer precipitation. *Clim. Dynam.* 51, 4271–4286. <https://doi.org/10.1007/s00382-017-3925-1>.
- Chen, Q., Sheng, L., Gao, Y., Miao, Y., Hai, S., Gao, S., Gao, Y., 2019. The effects of the trans-regional transport of PM<sub>2.5</sub> on a heavy haze event in the Pearl River Delta in January 2015. *Atmosphere* 10 (5), 237.
- Chu, D., Kaufman, Y., Ichoku, C., Remer, L., Tanré, D., Holben, B., 2002. Validation of MODIS aerosol optical depth retrieval over land. *Geophys. Res. Lett.* 29 (12) (MOD2-1-MOD2-4).
- Fast, J.D., Easter, R.C., 2006. A Lagrangian particle dispersion model compatible with WRF. 7th Annual WRF User's Workshop, pp. 19–22.
- Gadhavi, H.S., Renuka, K., Ravi Kiran, V., Jayaraman, A., Stohl, A., Klimont, Z., Beig, G., 2015. Evaluation of black carbon emission inventories using a Lagrangian dispersion model—a case study over southern India. *Environ. Pollut.* 15 (3), 1447–1461.
- Gao, Y., Zhang, M., Liu, Z., Wang, L., Wang, P., Xia, X., Tao, M., Zhu, L., 2015. Modeling the feedback between aerosol and meteorological variables in the atmospheric boundary layer during a severe fog-haze event over the North China Plain. *Atmos. Chem. Phys.* 15, 4279–4295. <https://doi.org/10.5194/acp-15-4279-2015>.
- Gao, M., Carmichael, G.R., Wang, Y., Saide, P.E., Yu, M., Xin, J., Liu, Z., Wang, Z., 2016. Modeling study of the 2010 regional haze event in the North China Plain. *Atmos. Chem. Phys.* 16, 1673–1691. <https://doi.org/10.5194/acp-16-1673-2016>.
- Gao, Z., Wang, X., Shen, L., Xiang, H., Wang, H., 2019. Observation and source apportionment of trace gases, water-soluble ions and carbonaceous aerosol during a haze episode in Wuhan. *Atmosphere* 10 (7), 397.
- Grell, G.A., Peckham, S.E., Schmitz, R., McKeen, S.A., Frost, G., Skamarock, W.C., Eder, B., 2005. Fully coupled “online” chemistry within the WRF model. *Atmos. Environ.* 39, 6957–6975.
- Gui, K., Che, H., Wang, Y., Wang, H., Zhang, L., Zhao, H., Zheng, Y., Sun, T., Zhang, X., 2019. Satellite-derived PM<sub>2.5</sub> concentration trends over Eastern China from 1998 to 2016: relationships to emissions and meteorological parameters. *Environ. Pollut.* 247, 1125–1133.
- Guo, S., Hu, M., Zamora, M.L., Peng, J., Shang, D., Zheng, J., Du, Z., Wu, Z., Shao, M., Zeng, L., Molina, M.J., Zhang, R., 2014. Elucidating severe urban haze formation in China. *Proc. Natl. Acad. Sci.* 111, 17373–17378.
- Han, R., Wang, S., Shen, W., Wang, J., Wu, K., Ren, Z., Feng, M., 2016. Spatial and temporal variation of haze in China from 1961 to 2012. *J. Environ. Sci.* 46, 134–146. <https://doi.org/10.1016/j.jes.2015.12.033>.
- Hong, S.Y., Noh, Y., Dudhia, J., 2006. A new vertical diffusion package with an explicit treatment of entrainment processes. *Mon. Weather Rev.* 134, 2318–2341.
- Hsu, S.C., Liu, S.C., Tsai, F., Engling, G., Lin, I.I., Chou, C.K.C., Kao, S.J., Lung, S.C.C., Chan, C.Y., Lin, S.C., Huang, J.C., Chi, K.H., Chen, W.N., Lin, F.J., Huang, C.H., Kuo, C.L., Wu, T.C., Huang, Y.T., 2010. High wintertime particulate matter pollution over an offshore island (Kinmen) off southeastern China: an overview. *J. Geophys. Res.* 115, D17309. <https://doi.org/10.1029/2009JD013641>.
- Hu, R., Wang, H., Yin, Y., Chen, K., Zhu, B., Zhang, Z., Kang, H., Shen, L., 2018. Mixing state of ambient aerosols during different fog-haze pollution episodes in the Yangtze River Delta, China. *Atmos. Environ.* 178, 1–10.
- Huang, X., Ding, A., Gao, J., Zheng, B., Zhou, D., Qi, X., Tang, R., Ren, C., Nie, W., Chi, X., Wang, J., Xu, Z., Chen, L., Li, Y., Che, F., Pang, N., Wang, H., Tong, D., Qin, W., Cheng, W., Liu, W., Fu, Q., Chai, F., Davis, S.J., Zhang, Q., He, K., 2020. Enhanced secondary pollution offset reduction of primary emissions during COVID-19 lockdown in China. *Natl. Sci. Rev.*, nwaa137 <https://doi.org/10.1093/nsr/nwaa137>.
- Jiang, C., Wang, H., Zhao, T., Li, T., Che, H., 2015. Modeling study of PM<sub>2.5</sub> pollutant transport across cities in China's Jing-Jin-Ji region during a severe haze episode in December 2013. *Atmos. Chem. Phys.* 15 (10), 5803–5814.
- Kan, H., Chen, R., Tong, S., 2012. Ambient air pollution, climate change, and population health in China. *Environ. Int.* 42, 10–19. <https://doi.org/10.1016/j.envint.2011.03.003>.
- Kang, H., Zhu, B., Gao, J., He, Y., Wang, H., Su, J., Pan, C., Zhu, T., Yu, B., 2019. Potential impacts of cold frontal passage on air quality over the Yangtze River Delta, China. *Atmos. Chem. Phys.* 19 (6), 3673–3685.
- Le, T., Wang, Y., Liu, L., Yang, J., Yung, Y., Li, G., Seinfeld, J., 2020. Unexpected air pollution with marked emission reductions during the COVID-19 outbreak in China (preprint). *Science* <https://doi.org/10.1126/science.abb7431>.
- Li, J., Wang, Z., Huang, H., Hu, M., Meng, F., Sun, Y., Wang, X., Wang, Y., Wang, Q., 2013. Assessing the effects of trans-boundary aerosol transport between various city clusters on regional haze episodes in spring over East China. *Tellus B* 65 (1), 20052.
- Li, Z., Guo, J., Ding, A., Liao, H., Liu, J., Sun, Y., Wang, T., Xue, H., Zhang, H., Zhu, B., 2017. Aerosol and boundary-layer interactions and impact on air quality. *Natl. Sci. Rev.* 4 (6), 810–833.
- Mlawer, E.J., Taubman, S.J., Brown, P.D., Iacono, M.J., Clough, S.A., 1997. Radiative transfer for inhomogeneous atmospheres: RRTM, a validated correlated-k model for the longwave. *J. Geophys. Res. Atmos.* 102, 16663–16682.
- Morrison, H., Thompson, G., Tatarskii, V., 2009. Impact of cloud microphysics on the development of trailing stratiform precipitation in a simulated squall line: comparison of one- and two-moment schemes. *Mon. Weather Rev.* 137, 991–1007.
- Rosenfeld, D., Sherwood, S., Wood, R., Donner, L., 2014. Climate effects of aerosol-cloud interactions. *Science* 343, 379–380. <https://doi.org/10.1126/science.1247490>.
- Sauvage, B., Fontaine, A., Eckhardt, S., Aubry, A., Boulanger, D., Petetin, H., Paugam, R., Athier, G., Cousin, J.M., Darras, S., Nédélec, P., Stohl, A., Turquety, S., Cammas, J.P., Thouriet, V., 2017. Source attribution using FLEXPART and carbon monoxide emission inventories: SOFT-IO version 1.0. *Atmos. Chem. Phys.* 17, 15271–15292. <https://doi.org/10.5194/acp-17-15271-2017>.
- Seibert, P., Frank, A., 2004. Source-receptor matrix calculation with a Lagrangian particle dispersion model in backward mode. *Atmos. Chem. Phys.* 4, 51–63.
- Shen, L., Wang, H., Zhao, T., Liu, J., Bai, Y., Kong, S., Shu, Z., 2020. Characterizing regional aerosol pollution in central China based on 19 years of MODIS data: spatiotemporal variation and aerosol type discrimination. *Environ. Pollut.* 114556.
- Shi, X., Brasseur, G.P., 2020. The response in air quality to the reduction of Chinese economic activities during the COVID-19 outbreak. *Geophys. Res. Lett.* 47, 8.
- Stohl, A., 2003. A backward modeling study of intercontinental pollution transport using aircraft measurements. *J. Geophys. Res.* 108, 1–8. <https://doi.org/10.1029/2002jd002862>.
- Stohl, A., Forster, C., Frank, A., Seibert, P., Wotawa, G., 2005. Technical note: the Lagrangian particle dispersion model FLEXPART version 6.2. *Atmos. Chem. Phys.* 5, 2461–2474.
- Tan, C.H., Zhao, T.L., Cui, C.G., Luo, B.L., Zhang, L., Bai, Y.Q., 2015. Characterization of haze pollution over Central China during the past 50 years. *China Environ. Sci.* 35, 2272–2280 (in Chinese).

- Tao, M.H., Chen, L.F., Su, L., Tao, J.H., 2012. Satellite observation of regional haze pollution over the North China plain. *J. Geophys. Res. Atmos.* 117, D12203. <https://doi.org/10.1029/2012JD017915>.
- Tian, H., Liu, Y., Li, Y., Wu, C.H., Chen, B., Kraemer, M.U., Li, B., Cai, J., Xu, B., Yang, Q., Wang, B., Yang, P., Cui, Y., Song, Y., Zheng, P., Wang, Q., Bjornstad, N., Yang, R., Grenfell, T., Pybus, G., Dye, C., 2020. An investigation of transmission control measures during the first 50 days of the COVID-19 epidemic in China. *Science* 368 (6491), 638–642.
- Tie, X., Huang, R.J., Cao, J., Zhang, Q., Cheng, Y., Su, H., Chang, D., Poschl, U., Hoffmann, T., Dusek, U., Li, G., Worsnop, D.R., O'Dowd, C.D., 2017. Severe pollution in China amplified by atmospheric moisture. *Sci. Rep.* 7, 1–8. <https://doi.org/10.1038/s41598-017-15909-1>.
- Wang, Y., Ying, Q., Hu, J., Zhang, H., 2014. Spatial and temporal variations of six criteria air pollutants in 31 provincial capital cities in China during 2013–2014. *Environ. Int.* 73, 413–422.
- Wang, N., Ling, Z.H., Deng, X.J., Deng, T., Lyu, X.P., Li, T.Y., Gao, X.R., Chen, X., 2018. Source contributions to PM<sub>2.5</sub> under unfavorable weather conditions in Guangzhou City, China. *Adv. Atmos. Sci.* 35 (9), 1145–1159. <https://doi.org/10.1007/s00376-018-7212-9>.
- Wang, H., Li, J., Peng, Y., Zhang, M., Che, H., Zhang, X., 2019. The impacts of the meteorology features on PM<sub>2.5</sub> levels during a severe haze episode in central-east China. *Atmos. Environ.* 197, 177–189.
- Wang, C., Horby, P.W., Hayden, F.G., Gao, G.F., 2020a. A novel coronavirus outbreak of global health concern. *Lancet* 395 (10223), 470–473.
- Wang, P., Chen, K., Zhu, S., Wang, P., Zhang, H., 2020b. Severe air pollution events not avoided by reduced anthropogenic activities during COVID-19 outbreak. *Resour. Conserv. Recy.* 158, 104814.
- Wei, W., Wu, B.G., Ye, X.X., Wang, H.X., Zhang, H.S., 2013. Characteristics and mechanisms of low-level jets in the Yangtze River Delta of China. *Bound. Layer Meteorol.* 149 (3), 403–424.
- Wei, P., Ren, Z.H., Wang, W.J., 2015. Analysis of meteorological conditions and formation mechanisms of lasting heavy air pollution in eastern China in October 2014. *Res. Environ. Sci.* 28 (5), 676–683 (in Chinese).
- Xu, X., Zhao, T., Liu, F., Gong, S.L., Kristovich, D., Lu, C., Guo, Y., Cheng, X., Wang, Y., Ding, G., 2016. Climate modulation of the Tibetan Plateau on haze in China. *Atmos. Chem. Phys.* 16, 1365–1375. <https://doi.org/10.5194/acp-16-1365-2016>.
- Xu, C., Jiao, L., Zhang, B., Zhao, S., Yuan, M., Gu, Y., Liu, J., Tang, X., 2017. Spatial and temporal variability of the PM<sub>2.5</sub>/PM<sub>10</sub> ratio in Wuhan, Central China. *Aerosol Air Qual. Res.* 17, 741–751. <https://doi.org/10.4209/aaqr.2016.09.0406>.
- Yang, Y.R., Liu, X.G., Qu, Y., An, J.L., Jiang, R., Zhang, Y.H., Sun, Y.L., Wu, Z.J., Zhang, F., Xu, W.Q., Ma, Q.X., 2015. Characteristics and formation mechanism of continuous hazes in China: a case study during the autumn of 2014 in the North China Plain. *Atmos. Chem. Phys.* 15 (7), 10987–11029.
- Zhai, S., An, X., Liu, Z., Sun, Z., Hou, Q., 2016. Model assessment of atmospheric pollution control schemes for critical emission regions. *Atmos. Environ.* 124, 367–377.
- Zhang, X.Y., Wang, Y.Q., Niu, T., Zhang, X.C., Gong, S.L., Zhang, Y.M., Sun, J.Y., 2012. Atmospheric aerosol compositions in China: spatial/temporal variability, chemical signature, regional haze distribution and comparisons with global aerosols. *Atmos. Chem. Phys.* 12 (2), 779–799.
- Zhang, X., Sun, J., Wang, Y., Li, W., Zhang, Q., Wang, W., Quan, J., Cao, G., Wang, J., Yang, Y., Zhang, Y., 2013. Factors contributing to haze and fog in China. *Chin. Sci. Bull.* 58 (13), 1178–1187 (in Chinese).
- Zhang, F., Wang, Z.W., Cheng, H.R., Lv, X.P., Gong, W., Wang, X.M., Zhang, G., 2015. Seasonal variations and chemical characteristics of PM<sub>2.5</sub>, in Wuhan, Central China. *Sci. Total Environ.* 518, 97–105.
- Zhang, Y., Ding, A., Mao, H., Nie, W., Zhou, D., Liu, L., Huang, X., Fu, C., 2016. Impact of synoptic weather patterns and inter-decadal climate variability on air quality in the North China Plain during 1980–2013. *Atmos. Environ.* 124, 119–128. <https://doi.org/10.1016/j.atmosenv.2015.05.063>.
- Zhao, X.J., Zhao, P.S., Xu, J., Meng, W., Pu, W.W., Dong, F., He, D., Shi, Q.F., 2013. Analysis of a winter regional haze event and its formation mechanism in the North China Plain. *Atmos. Chem. Phys.* 13, 5685–5696. <https://doi.org/10.5194/acp-13-5685-2013>.
- Zheng, S., Pozzer, A., Cao, C., Lelieveld, J., 2015. Long-term (2001–2012) concentrations of fine particulate matter (PM<sub>2.5</sub>) and the impact on human health in Beijing, China. *Atmos. Chem. Phys.* 15 (10), 5715–5725.
- Zheng, H., Kong, S., Wu, F., Cheng, Y., Niu, Z., Zheng, S., Yang, G., Yao, L., Yan, Q., Wu, J., 2019. Intra-regional transport of black carbon between the south edge of the North China Plain and central China during winter haze episodes. *Atmos. Chem. Phys.* 19, 4499–4516.
- Zheng, H., Kong, S., Chen, N., Yan, Y., Liu, D., Zhu, B., Xu, K., Cao, W.X., Ding, Q.Q., Lan, B., Zhang, Z.X., Zheng, M., Fan, Z., Cheng, Y., Zheng, S., Yao, L., Bai, Y., Zhao, T., Qi, S., 2020. Significant changes in the chemical compositions and sources of PM<sub>2.5</sub> in Wuhan since the city lockdown as COVID-19. *Sci. Total Environ.* 140000.
- Zhu, Q., Liu, Y., Jia, R., Hua, S., Shao, T., Wang, B., 2018. A numerical simulation study on the impact of smoke aerosols from Russian forest fires on the air pollution over Asia. *Atmos. Environ.* 182, 263–274.